Journal of Membrane Science 524 (2017) 436–448

Contents lists available at ScienceDirect

Journal of Membrane Science

journal homepage: www.elsevier.com/locate/memsci

# Molecular simulations of polyamide membrane materials used in desalination and water reuse applications: Recent developments and future prospects

Harry F. Ridgway[a,b,*], John Orbell[a], Stephen Gray[a]

[a] Institute for Sustainability and Innovation, Victoria University, Building 4 (via gate 3), Room 4103 Werribee Campus, Hoppers Lane, Werribee 3030, Australia

[b] AquaMem Scientific Consultants, Rodeo, NM, USA

## ARTICLE INFO

*Keywords:*
Computational chemistry
Molecular modeling
Polyamide membranes
Reverse osmosis
Nanofiltration
Water treatment
Desalination
Solute rejection
Membrane flux
Biofouling
Biofilm
Membrane transport
Membrane fouling
Water reuse

## ABSTRACT

Desalination and water reuse are rapidly evolving technologies that have become mainstays of a broad portfolio of water management practices around the globe. Osmotically-driven molecular partitioning processes mediated by functional permselective membranes lay at the heart of each of these technologies. Despite a strong theoretical and empirical framework of knowledge discovered over the past half century that allows engineering of modern reverse osmosis (RO) systems at unprecedented scales, our understanding of water transport and solute rejection at the atomic and molecular scales by the semipermeable membranes is incomplete. One reason for this is a dearth of analytical techniques capable of non-invasively accessing (and visualizing) in real time the exceedingly small spatial and temporal dimensions of atomic interactions underlying membrane transport phenomena. This knowledge gap has been increasingly eroded, however, since the first use of molecular simulations to explore RO membrane structure and dynamics in the late 1990s. Over the last decade, molecular dynamics (MD) and related simulations techniques have been aggressively pursued to advance understanding of membrane architecture and transport at the atomistic scale. Results emerging from sophisticated computational approaches, especially when coupled with today's powerful new imaging technologies, reveal a rich landscape of physicochemical interactions not only inside the polymer membranes, but also at the water-membrane interface. For example, it is now clear that the discriminating polyamide (PA) layer of modern RO membranes consists of an inhomogeneous tangled polymer network pervaded by tortuous water-filled transmembrane “tunnels” and nanopores whose shapes fluctuate at ambient temperatures over femtosecond to picosecond time scales. Recent modeling efforts indicate that the nanoscale roughness of PA membranes, evident in electron micrographs, is also reflected at the atomic scale, with an ill-defined diffuse interfacial region shared with the bulk water phase. Simulations are also yielding a clearer picture of water and solute (ions and small organics) behaviors inside the membrane matrix resulting from

*Abbreviations:* Å, Angstrom; AFM, atomic force microscopy; AMBER, Assisted Model Building and Energy Refinement R. Salomon-Ferrer, D.A. Case, R.C. Walker, An overview of the Amber biomolecular simulation package, WIREs Comput. Mol. Sci. 3 (2012) 198–210; BSA, Bovine serum albumin; CA, cellulose acetate; CHARMM, Chemistry at Harvard Molecular Mechanics, MD code originally developed by Martin Karplus, Harvard University; CN, cellulose nitrate; CNT, carbon nanotube; CVFF, Consistent Valence Force Field P. Dauber-Osguthorpe, V.A. Roberts, D.J. Osguthorpe, J. Wolff, M. Genest, A.T. Hagler, Structure and energetics of ligand binding to proteins: E. coli dihydrofolate reductase-trimethoprim, a drug-receptor system, Proteins: Structure, Function and Genetics 4 (1988) 31–47; GROMACS, Groningen Molecular Simulation package; LAMMPS, Large-scale Atomic/Molecular Massively Parallel Simulator; MD, molecular dynamics; MPa, 1 million Pascals≈10 atm≈150 psi; MPD, meta-phenylenediamine; NAMD, Nanoscale Molecular Dynamics MD code developed at Theoretical and Computational Biophysics Group at University of Illinois at Urbana–Champaign.; NEMD, Non-equilibrium molecular dynamics; NF, nanofiltration; NMR, nuclear magnetic resonance; ns, nanosecond; OPLS-AA, Optimized Potential for Liquid Simulations – All Atom W.L. Jorgensen, D.S. Maxwell, J. Tirado-Rives, Development and Testing of the OPLS All-Atom Force Field on Conformational Energetics and Properties of Organic Liquids, J. Am. Chem. Soc. 118 (1996) 11225–11236.; PA, polyamide; PALS, positron annihilation lifetime spectroscopy; ps, picosecond; RBS, Rutherford backscattering spectrometry; RDF, Radial distribution function; RO, reverse osmosis; SD, Solution Diffusion Theory of: H.K. Lonsdale, U. Merten, R.L. Riley, Transport properties of cellulose acetate osmotic membranes, J. Appl. Polym. Sci. 9 (1965) 1341–1362.; SEM, scanning electron microscopy; SMD, steered molecular dynamics a user interactive form of MD in which the viewer can actively manipulate selected molecules in the system by pulling or dragging; SPC, flexible simple point charge water model of K. Toukan, A. Rahman, Molecular-dynamics study of atomic motions in water, Phys. Rev. B. 31 (1985) 2643–2648.; TEM, transmission electron microscopy; TIP3P, Flexible water model of: W.L. Jorgensen, J. Chandrasekhar, J.D. Madura, R.W. Impey, J. Klein, Comparison of simple potential functions for simulating liquid water, J. Chem. Phys. 79 (1983) 926–935.; TIP4P-Ew, re-parameterized TIP4P water model for Ewald techniques H.W. Horn, W.C. Swope, J.W. Pitera, J.D. Madura, T.J. Dick, G.L. Hura, T. Head-Gordon, Development of an improved four-site water model for biomolecular simulations: TIP4P-Ew, J. Chem Physics 120 (2004) 9665.; TFC, thin-film composite membrane; TMC, benzene-1,3,5-tricarbonyl chloride (trimesolyl chloride); TMD, targeted molecular dynamics a user interactive form of MD in which the viewer can actively manipulate selected molecules in the system by pulling or dragging; VDW, Van der Waals; XPS, x-ray photoelectron spectrometry

* Correspondence to: PO Box 251, Rodeo, New Mexico, 88056 USA.
*E-mail address:* ridgway@vtc.net (H.F. Ridgway).

http://dx.doi.org/10.1016/j.memsci.2016.11.061
Received 10 October 2016; Received in revised form 21 November 2016; Accepted 23 November 2016
Available online 25 November 2016
0376-7388/ © 2016 Elsevier B.V. All rights reserved.

complex intermolecular hydrogen bonding and atomistic solvation processes. The thermodynamic (enthalpy and free-energy) barriers to water and solute entrance into nanopores located at membrane surfaces have been recently elucidated by means of specialized non-equilibrium simulations protocols. Notwithstanding these recent successes, questions nonetheless remain concerning membrane molecular organization and performance, especially with respect to their ability to reject certain small organic compounds and not others. Other questions concern the dynamic interplay between membrane surfaces and foulant molecules as they undergo adsorption. Because of its unique ability to translate atomic-scale interactions and processes into a dynamic visual experience, it is anticipated that computational chemistry will play an ever greater role in the coming years in helping to answer these and related questions about membrane structure and function. It is expected that fundamental advancements in these areas will lead to a new generation of membrane materials with improved durability and reduced energy demands.

## 1. Background and introduction

Reverse osmosis (RO) is currently the most widely accepted demineralization method for large-scale seawater desalination and water reclamation activities around the globe. More than half a century ago, Reid and Breton [1] and Reid and Kuppers [2] first demonstrated that cellulose acetate (CA) polymers exhibited salt rejection and thus was thought to be a promising candidate for carrying out desalination. The water fluxes of the early CA membranes were, however, too low to be economically viable. Working at UCLA in 1959–1960, Loeb and Sourirajan [3] reported the discovery of the first practical (*i.e.*, high flux) RO membrane, comprised of an asymmetrically structured cellulose acetate (CA) film. Cellulose acetate membranes are produced by a phase-inversion process first commercialized at Gulf General Atomic, San Diego, California, USA in the early 1960s [4]. By 1962 it was recognized that salt rejection occurred in a thin dense discriminating ("skin") layer on the feed surfaces of CA membranes [5]. This pivotal observation quickly led to the concept of the thin-film composite (TFC) membrane design in which an active semipermeable barrier is physisorbed onto a mechanically durable high-porosity support layer.

The first TFC membranes were engineered in the early 1960s by Francis and Cadotte at North Star Research Institute, Minneapolis, Minnesota, USA. The early TFC membranes consisted of thin CA films cast on water, which were subsequently transferred onto porous polysulfone (PS) supports. Concomitantly, researchers at General Atomic prepared films as thin as 300 Å on glass plates by the Carnell-Cassidy method [6]. These were floated onto water and then transferred onto porous CN/CA supports (R.L Riley, Separation Systems Technology, Inc., personal communication). By the mid-1960's Rozelle and co-workers, also at North Star Research, prepared TFC membranes consisting of a thin (about 250 nm) permselective polyamide (PA) film cast onto a porous PS support [7]. The PA membranes were formed by interfacial polycondensation of an aqueous amine reacted with hexane-diacyl chloride, an organic-soluble difunctional acid chloride.

The first commercial TFC membrane was the PA-300 developed by Riley et al. at UOP Fluid Systems Division in 1975 for military RO water purification units (ROWPUs). The membrane was formed interfacially on a PS support by the reaction of polyepiamine with isophthaloyl chloride. Subsequently, the first TFC membrane to be utilized in a large scale commercial desalination facility in Jeddah, Saudi Arabia in 1977 was the RC100 membrane, which was formed by the interfacial reaction of polyepiamine with toluene diisocyanate.

The PA-300 was superseded in the late-1970s by the fully aromatic crosslinked PA membrane developed by Cadotte et al. working at North Star Research [8,9]. The so-called "Cadotte" membrane is formed by the interfacial reaction of *meta*-phenylene diamine (MPD) with trimesolyl chloride (TMC; benzene-1,3,5-tricarbonyl chloride) and today remains the state-of-the-art workhorse for desalination and reuse applications around the world (Fig. 1).

While numerous incremental advancements have been made in PA

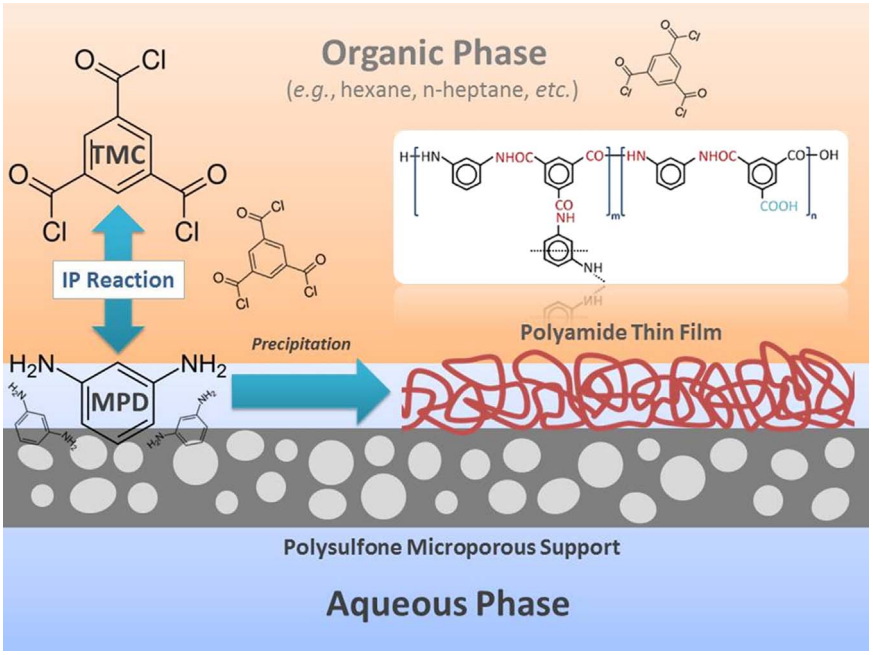



**Fig. 1.** Schematic of general synthesis protocol for preparation of the "Cadotte" polyamide TFC membrane. TMC and MPD residues undergo interfacial polymerization at an organic/aqueous interface leading to precipitation of a thin insoluble PA film on the surface of a microporous polysulfone structural support.

membrane performance and durability over the past several decades, understanding of membrane structure and function at the molecular and atomic scales has not evolved as rapidly. The solution-diffusion (SD) theory described by Merten [10] and Lonsdale et al. [11] provided the first reliable (and still widely accepted) theoretical treatment of the subject of water flux and solute rejection by RO membranes [12]. However, SD theory has contributed little in terms of relating membrane structure and dynamics at the nano- and molecular scales to the actual chemical basis for water and solute transport mechanisms. Only over the past decade or so have powerful new analytical and imaging technologies emerged that allow direct probing of membrane molecular architecture and structural dynamics [13].

For example, it has been recently demonstrated that the rough peaks (*i.e.*, protuberances) that can be visualized at the surfaces of PA membranes by transmission electron microscopy (TEM) and atomic-force microscopy (AFM; see Fig. 2) are in fact hollow water-filled voids rather.

than dense polymer [14], which helps to explain the high relative water fluxes of modern PA membranes. Pacheco et al. [15,16] reported the use of 3D TEM tomography to reveal the hollow nature of the protuberances and develop correlations between protuberance wall thicknesses and water flux. To a large extent, the nano-scale surface morphometry, thickness and performance of PA membranes can be controlled by varying the ratio of MPD to TMC and other process variables during interfacial polymerization [17,18]. Together these and other recent studies indicate that solute partitioning takes place across PA discriminating layers much thinner than previously envisioned, perhaps no more than 5–10 nm in thickness [18]. These dimensions fall well within the range that can be modeled at the fully atomistic level by modern computational methods.

Other experimental and analytical techniques have recently begun to shed light on how water and solutes (*e.g.*, ions and small organics) undergo transport across RO membranes at the molecular and atomic scales. In a recent review, Fujioka and co-workers [19] reported how positron annihilation lifetime spectroscopy (PALS) has been used to determine the mean free-volumes and nanopore radii (0.20–0.29 nm) of commercial RO membranes, which is correlated with small-molecule rejection and water flux. Using X-ray photoelectron spectrometry (XPS) and Rutherford backscattering spectrometry (RBS), Coronell et al. [20] found that RO (ESPA3) and nanofiltration (NF90) membranes were either chemically homogeneous or heterogeneous, respectively, as a function of the depth of the PA discriminating layer. By quantifying $pK_a$ distributions of carboxyl groups (-R-COOH), the degree of polymer crosslinking, barium-probe concentration, and $Ba^{2+}$ ion interaction potentials, the NF90 near-surface region was found to be chemically distinct from the average (bulk) membrane values. These data inferred relatively larger nanopores near the NF90 surface, although no correlation was observed with AFM surface roughness. A similar asymmetric void distribution was directly visualized in polyamide RO membrane thin films by Pacheco et al. [15,16]. Additional RBS studies demonstrated that only a fraction (0.40–0.81) of the free (*i.e.*, non-crosslinked) carboxylate groups (-R-COO-) in the PA membrane are accessible to $Ba^{2+}$ ions, and that this fraction is largely independent of bulk solution pH [21,22]. Such findings support the notion that RO and NF membranes are chemically and structurally heterogeneous materials, and that their flux and rejection characteristics must be strongly influenced and controlled by localized internal environments.

Currently there are few analytical techniques aside from x-ray crystallography and perhaps nuclear magnetic resonance (NMR) that have sufficient spatial and temporal resolution to explore and monitor water, solute and foulant molecule interactions with membrane materials at the atomic scale. Such interactions can, however, be successfully probed in abundant detail by means of modern computational chemistry and statistical-mechanical approaches, which can readily access spatial and temporal regimes well below most analytical methods. For this reason, computational methods have been increasingly employed in recent years to elucidate and quantify dynamic atomistic-scale mechanisms and processes in functional membrane materials (see Ridgway et al. [23]).

Recently, Elbro et al. [24] reviewed the basic principles of MD simulations as they apply to a wide range of membrane materials used in water treatment applications, including carbon nanotubes and polymers other than PA. In contrast to the Elbro review, the current work is narrowly focused on PA-based membrane materials, including RO and NF membranes, primarily because of the enormous commercial impact these materials have had across the water treatment community. It should be stressed that both RO and NF membrane materials may be fabricated by interfacial polymerization of MPD and TMC; and depending on process conditions, a finished PA membrane can exhibit physical and separation properties characteristic of an RO membrane, such as high solute rejection and a denser (and often thicker) barrier layer compared to less dense (“loose”) NF membranes exhibiting lower solute rejections and high fluxes. At the molecular scale, however, both RO and NF membranes share strong similarities in terms of randomized (non-crystalline) polymer arrangement, crosslinking frequencies and nanopore motifs.

The purpose of this review is to provide a current overview of what has been learned about RO membrane structure and dynamics through the lens of modern molecular simulations techniques. The review is not intended to be an exhaustive analysis of the vast literature regarding RO membranes and/or computational chemistry in general, but rather

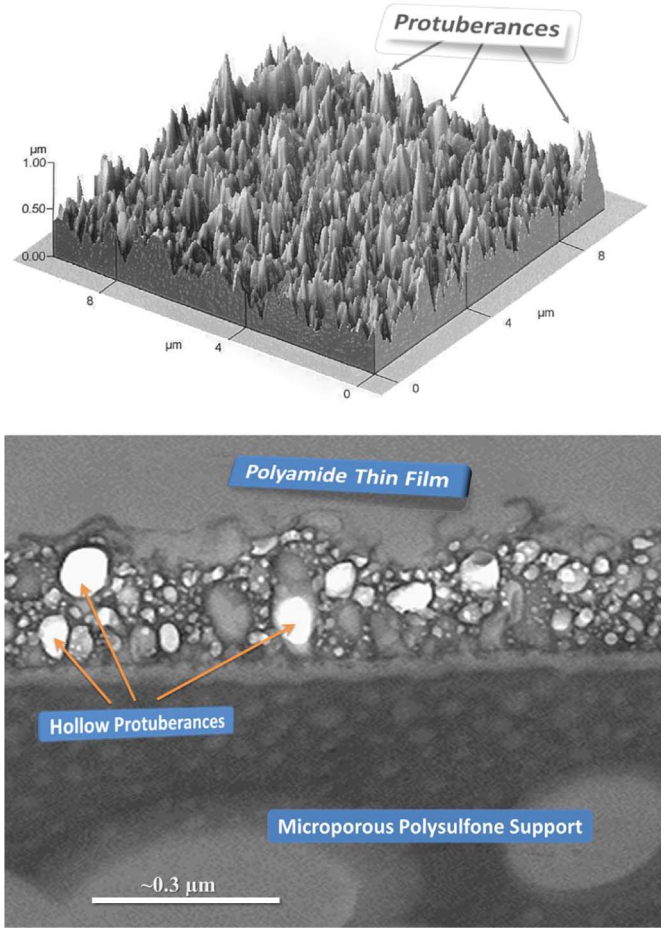



**Fig. 2.** AFM and TEM images of polyamide TFC membranes showing rough surface morphology and hollow protuberances (unpublished images provided courtesy of Bob Riley, Separation Systems Technology, San Diego, California, USA). The structural variations seen in the PA discriminating layer make it challenging to know what area to model.

**Table 1**
Summary of some relevant membrane molecular modeling studies performed since the late 1990s.

| Polymer system | Algorithm | MD code | Prot. | Density (g/cm$^3$) | wt% $H_2O$ | Water $\boldsymbol{D}_{mem}$ ($10^{-9}$m$^2$/s) | | $H_2O$ Model | Mechanism | Reference |
|---|---|---|---|---|---|---|---|---|---|---|
| PA | CB+RxL[a] | CVFF (BioSym) | Yes | ~1.3 | ~23 | 0.20 | ~10 | CVFF | Jump[c] | Kotleyanskii et al. [26,33] |
| PA | RMSB[b] | CHARMM | NR[e] | ~1.4 | ~23 | 0.50 | ~10 | TIP3P | (Jump for for Na+ & Cl-)NR for water | Harder et al. [31]; Luo et al. [38] |
| PA | CCA Course Grain | CCA model | NA[i] | | NA | NA | NA | NA | NA | Oizerovich-Honig et al. [25] |
| PA | CB+RxL | DLPOLY/OPLS-AA | Yes | ~1.34 | ~23 | 0.21 | ~10 | TIP4P-Ew | NR | Hughes and Gale [44,58] |
| PA | RMSB | GROMACS | Y/N | ~1.30 | 26–29 | 0.50 | ~10 | TIP3P & SPC | NR | Kolev and Freger [27,28] |
| PA | CB+RxL | DLPOLY/AMBER99 | Yes | ~1.32 | 23 | 2.4 for pockets; 0.2 for confined | ~10 | TIP4P/2005 | Smooth[d] | Ding et al. [39,40] |
| PA | RMSB | NAMD[j]/GAFF[k]/NEMD[l] | Yes | ~1.38 | NR | NR | NR | ? | Jump | Shen et al. [32,48] |
| PA/nxL[h] | CB-NxL[f] | LAMMPS/CVFF | No | ~1.38 | 23 | 0.12 | ~10 | CVFF | NR | Xiang et al. [41] |
| PA | CB+RxL | LAMMPS/CVFF | No | ~1.35 | NR | NR | NR | CVFF | NR | Xiang et al. [42] |
| PES | ACB[g] | Cerius2/CVFF/CLAYFF | NR | ~1.30 | | 1.33 (near surface) | ~1.8 | CVFF | NR | Ahn et al. [59] |
| PA/Si Wafer | mLbL[l] | ? | Yes | NR | NR | NR | NR | NA | NA | Liyana-Arachchi et al. [52] |
| PA/CNT | CB+xL[m] | DLPOLY/NVT | Yes | NR | NR | 3.38 (for bulk water) 3.07 (proximal to CNT) | NR | SPC/E | NA | Araki et al. [51] |
| PA/nxL | CB+NxL | CHARMM27/PCFF | NR | 0.6–1.5 | NR | 2.13 @ 1.06 density 0.1 @ 1.40 density | NR | NR | Jump | Gao et al. [30] |

[a] CB+RxL=Initial chain built over a randomly-folded self-avoiding lattice; or initial grouped linear chains; separate random crosslinking (RCL) step.
[b] RMSB=Randomized monomer solution bonding followed by MPD "flooding" to maximize crosslinking.
[c] Jump=Water diffusion characterized by sudden jumps or hops from one low-energy domain inside membrane to another adjacent domain.
[d] Smooth=Obvious water jumps were not observed over the MD time scales used.
[e] NR=Either not calculated or not reported.
[f] CB+NxL=Grouped chains with no crosslinking.
[g] ACB=Amorphous chain builder.
[h] PA/nxL=Non-crosslinked PA membrane.
[i] NA=Not applicable.
[j] GAFF=Generalized Amber force field.
[k] NEMD=Non-equilibrium molecular dynamics.
[l] NAMD=Nanoscale Molecular Dynamics program, Theoretical and Computational Biophysics Group, University of Illinois at Urbana–Champaign.
[m] CB+xL=chain extension followed by separate crosslinking steps.

specifically focuses on molecular modeling studies, primarily at the atomistic scale, of PA and some related membranes that have been performed since the late 1990 s. The main objective of the review is to identify common trends among the results of the modeling studies that have been undertaken to date. In addition, the review will provide some ideas about the possible future applications of molecular simulations in membrane research and development and the kinds of questions it might address.

## 2. Molecular simulations of water and salt transport in polyamide reverse osmosis membrane materials

Table 1 provides a brief summary of most of the molecular modeling studies that have been conducted to date aimed at understanding the structural dynamics and transport characteristics of permselective PA (and a few related) membrane materials. Nearly all of the molecular modeling efforts reviewed herewith were performed at the fully atomistic scale. The sole exception was the study reported by Oizerovich-Honig, et al. [25] in which a coarse-grained modeling approach was employed aimed at advancing understanding of the interfacial polymerization process itself.

The first detailed molecular dynamics (MD) study of a crosslinked PA membrane closely resembling Dow Filmtec's flagship FT30 membrane was reported by Kotelyanskii and co-workers [26]. Membrane models in that study were built over a linear, randomly-folded self-avoiding lattice that was subsequently decorated with alternating MPD and TMC monomeric units (residues) and annealed by standard NVT equilibrium MD protocols (Fig. 3). Explicit flexible water molecules, modeled according to the CVFF force field, were randomly inserted into the structure at the appropriate degree of solvation (about 23 wt% for the solvated membrane). The system was energy minimized at a final density of about 1.38 g/cm$^3$. It is noteworthy that in this and some other later studies, non-crosslinked TMC residues were modeled in the wholly protonated form, which presumably would only exist in practice at pH values well below the p$K_a$ of the free (dangling) carboxylic acid groups. At feedwater pH values typically encountered in actual desalination facilities (*e.g.*, 6.5–8.5), any free (*i.e.*, non-crosslinked) carboxylic acid groups in the membrane would be expected to exist primarily in the ionized form (-R-COO-), necessitating the presence of dissolved cations (*e.g.*, $Na^+$, $Ca^{2+}$, $Mg^{2+}$, *etc.*) distributed appropriately in the models to maintain system charge neutrality. Despite this expectation, Coronell et al. [21,22] nevertheless experimentally demonstrated using RBS spectrometry that there are dual p$K_a$ values (located at pH 5.23 and 8.97) for carboxylic acid groups occupying commercial FT30 membranes. Thus, it seems that at least some indefinite portion of these groups could remain protonated under normal plant operating conditions.

Currently, very little is known about how the degree of –R-COOH protonation, as well as the nature and concentration of any counterions present, might influence PA membrane structure and function at the molecular scale. Kolev and Freger [27,28] prepared PA membrane models in the neutral and fully ionized states, and they were able to show reductions in water and solute ($Na^+$) free diffusion in their non-protonated models. These findings may have implications for how actual RO plants are operated for modern water-reuse applications. For example, there is sometimes a desire on the part of facility managers to increase the RO feedwater pH, ostensibly to lower the cost of acid addition, which is substantial in large plants. At the same time, however, there is apprehension that raising pH levels (*e.g.*, from 6.8 to 7.2) would compromise rejection of certain trace organics of public health concern, such as nitrosodimethylamine (NDMA).

Kotelyanskii and co-workers [26] introduced sodium and chloride atoms at random loci throughout their neutral PA models at concentrations of about 0.1–0.2 wt% of water. Intra-chain crosslinks were

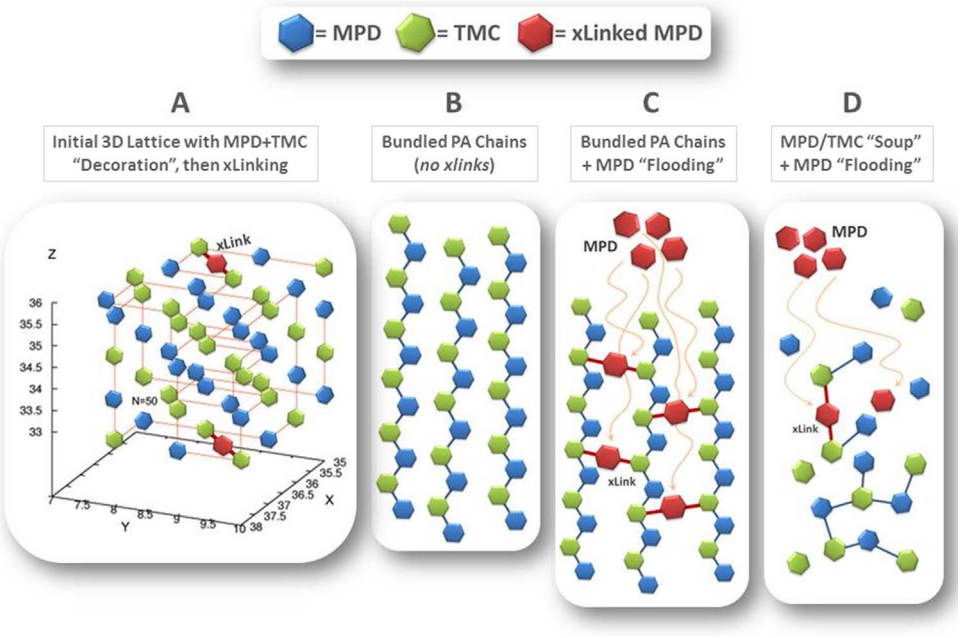



**Fig. 3.** Schematic depicting four generalized strategies that have been employed by different research groups to prepare PA membrane models. These and related PA build approaches have been discussed in a previous review by Ridgway et al., [23]. **Panel A:** "Markov Chain" approach to build an initial linear randomly-folded self-avoiding chain that is subsequently "decorated" with alternating MPD and TMC residues. Crosslinks are introduced in a separate step. This general scheme has been used by Kotelyanskii et al., [26,33]. **Panel B:** Grouping of pre-built linear PA chains with no crosslink bonding. Though depicted as linear chains here, following energy minimization, such chains rearrange to form an amorphous matrix (*cf.*, Xiang et al. [41]). **Panel C:** Grouping of pre-built linear PA chains with crosslink bonding introduced in successive "MPD flooding" stages. MPD residues may be introduced before or after chain optimization. A distance heuristic is used to control crosslink bonding events between proximal TMC residues This general scheme has been used by Hughes and Gale [44] and Xiang et al. [42,43]. **Panel D:** Randomized bonding over an energy-minimized "soup" of MPD and TMC residues. Chain growth occurs randomly from many initial loci creating small aggregates that gradually coalesce into the PA network. A distance heuristic is used to control PA bonding. Successive MPD flooding events are used to drive PA chain bonding (and crosslinking) toward completion. Although a "crosslink" point is indicated by a label (xLink), no distinction is made between crosslinking and chain growth in this scenario. This "progressive crosslinking" approach, first introduced by Harder et al. [31], has been widely adopted with modifications by others.

introduced into some of their model systems by "bridging" the carboxylic acid groups of TMC units separated by $< 7 \pm 2$ Å with newly introduced MPD residues. This and other PA model building strategies are summarized in Fig. 3. Following energy minimization (relaxation) of the systems to assure an amorphous polymer network, constant-temperature (NVT) molecular dynamics was performed for periods of up to 5 ns. The Kotelyanskii models clearly displayed reduced water (about $0.20\times10^{-9}$ $m^2/s$) and ion diffusivities within the membrane interiors (about 10x less compared to bulk solution values), which they surmised were mainly responsible for salt rejection across the membrane.

Perhaps the most significant finding in this early simulations study was that water diffused through the membranes by a "jumping" or "hopping" mechanism in which individual water molecules undergo a sudden (nearly instantaneous) translocation between adjacent low-energy nanopores in response to local chain rearrangements or abrupt (thermally-inspired) kinetic inputs from water-water or water-membrane collision dynamics. Such a jump mechanism is similar to that described previously for dissolved gas molecules in glassy amorphous polymer systems [29]; and it has now been well documented in later membrane modeling studies [30–32]. The characteristic jump length was about 3 Å for crosslinked or linear (*i.e.*, non-crosslinked) PA systems, while the average time between jumps was about 1–2 ns. The authors observed a lower mobility for $Cl^-$ ions relative to $Na^+$ ions inside the hydrated polymer network, which was attributed to polar groups on the polymer chains (*e.g.*, carbonyl oxygens on amide bonds) that participate in preferential anion solvation. Solvation of $Na^+$ ions inside the membrane was similarly assisted by replacement of one of the normally hydrating water molecules for this ion with a polar carbonyl oxygen (-R–C=O) from the polymer. It was additionally observed that > 90% of water molecules in the solvated polymer formed an interconnected (*i.e.,* hydrogen-bonded) continuum phase or "percolating network" through which water molecules could migrate. Thus, when water transits the membrane under an applied differential pressure, there should be a significant thermodynamic penalty associated with breakage of water-water hydrogen bonds, particularly for those water molecules undergoing jump-type displacements from one local low-energy domain (*e.g.*, a water-filled nanopore) to another. This de-solvation penalty has since been demonstrated in later PA membrane modeling studies by other researchers (see below).

The water jump mechanism was confirmed in a follow-up MD study by Kotelyanskii et al. [33] wherein the average jump length was found to be essentially independent of the type of system studied (*i.e.*, linear *versus* crosslinked) and instead was believed to be coupled to cooperative rearrangements of water molecules within the nanoporous membrane voids. On the other hand, the jump frequency, which effectively regulated the rate of water diffusion across the membrane, varied with polymer dynamics, crosslink density and hydrogen bonding interactions.

Recent efforts have been made to model PA membranes and their formation dynamics using course-grained simulations strategies, in which monomers are no longer considered at the atomistic scale where individual atoms are explicitly represented, but rather as atom aggregates that form a single interacting unit [34]. One such approach was reported by Oizerovich-Honig and co-workers at the Technion University, Israel [25]. These researchers used the so-called "cluster-cluster aggregation" (CCA) model, which was previously developed by Meakin et al. [35] to emulate porous media. Use of a course-grained method allowed the researchers to move beyond mean field approximation predictions to explore PA film formation and structure. In this model, MPD and TMC residues were represented as "soft" spherical particles similar in size, σ, with a maximum allowable overlap of 0.9σ. The trifunctional TMC monomers can bind only to MPD's, and the MPD's only to TMC's. The simulations were initiated by random placement of residues in separate halves of a 3D asymmetric box, representing the organic and aqueous phases. Water was not added explicitly, but instead represented by its effects on particle partitioning. Results indicated exceedingly rapid percolating film formation ( < 20 μs) leading to a rough porous surface (and interior), a prominent nanoscale hallmark of PA membranes [14–16,36]. By introducing a bond spring constant ($k$) between particles, membrane permeation could be readily controlled, with essentially rigid membranes ($k > 20$) exhibiting 10-fold lower (particle) fluxes compared to flexible models ($k < 5$). As is the case when synthesizing actual PA thin films [18,22,37], the overall properties of the continuum models, including permeability, pore distribution, surface roughness, density, and diffusion characteristics, could be regulated by manipulating the MPD/TMC residue ratio and particle interaction potentials.

Using a membrane building approach that differed fundamentally from those described above (Fig. 3), Harder et al. [31] and Luo et al. [38] constructed PA membrane models that yielded reasonable estimates of water flux ($1.4\times10^{-6}$ m/s) and salt (NaCl) rejection (99.9%) given a (calculated) 3 MPa applied pressure differential and a 0.125 μm width membrane. Their models were constructed according to a somewhat novel algorithm in which randomized covalent bonding events were carried out over an energy-minimized solution or "soup" of free MPD and TMC monomeric units. As the concentrations of free MPD and TMC residues diminished over time (due to polymerization), additional free MPD units were "flushed" into the system at intervals to gradually maximize (*i.e.,* saturate) crosslinking opportunities between TMC neighbors closer than some user-defined bond distance heuristic (Fig. 3). This "progressive crosslinking" strategy resulted in amorphous polymer networks that exhibited densities close to experimentally observed values (about 1.38 $g/cm^3$). Water was introduced into the dry polymer matrices by extended MD equilibration against liquid water reservoirs (TIP3P water model). Using their models in NVT equilibrium MD simulations, Luo et al. [38] reported there was no discernable energy barrier for $Na^+$ or $Cl^-$ ions as they approached and began to diffuse into the membrane matrix. This was confirmed by non-equilibrium "targeted molecular dynamics" (TMD), in which individual ionic species were interactively "pulled" or "dragged" across the membrane interior. Irregular spikes in the applied TMD "dragging" force along the trajectories indicated that $Na^+$ ions, but not $Cl^-$ ions, exhibited a 'hopping' transport mechanism similar to that first described by Kotelyanskii et al. [26,33]. The TMD simulations also directly revealed contiguous transmembrane pathways for water or ion passage extending from the feed surface to the permeate side of the membrane. The presence of such pathways appears to be consistent with the "continuous percolating network" of hydrogen-bonded water molecules described by Kotleyanskii et al. [26,33].

Because it may more closely resemble the interfacial synthetic route used to make actual PA membranes, modifications of the "progressive-crosslinking" building algorithm first described by Harder et al. [31] have been adopted in a number of subsequent MD simulations studies to investigate PA nanostructure, water and solute transport behaviors [27,28,32,39,40], as well as biofoulant adsorption processes [41–43].

More-or-less concurrent with the Harder and Luo studies described above [31,38], Hughes and Gale [44] constructed PA membrane models in a manner similar to that described by Kotelyanskii and co-workers [26,33] in which chain elongation and bundling of 24 linear polymers was carried out prior to a separate crosslinking step. However, these authors additionally included in their systems a layer of specially parameterized *pseudo*-carbon atoms that bounded the PA membrane. According to the authors, this additional layer approximated a course-grained model of the polysulfone support part of the TFC membrane, which had been neglected in previous atomistic models. Atoms in the layer had no partial charge and were assigned Van der Waal's (VDW) parameters for an aliphatic carbon in the OPLS-AA force field (*i.e.* σ=3.5 Å, ε=2.76 kJ/mol); and they were tethered by a sizable harmonic potential (bond constant=419 kJ/mol). In accordance with the earlier observations of Kotelyanskii et al. [26,33] and Harder et al. [31], Hughes and Gale [44] reported that, for their non-

pressurized models, water inside the membrane exchanged with the bulk phase at a rate of about 149 molecules/ns; and diffusivities of water were reduced nearly 10-fold inside the membrane, which was similar to what the earlier modeling studies had revealed. It was also found that water molecules in the membrane formed into pockets or voids that were interconnected to one another by narrow tortuous tunnels containing single-file chains of water molecules hydrogen bonded to each other, which is similar to observations made by Kotelyanskii et al. [26,33] and Ding et al. [39]. A diffusion rate reduction was also observed for $Na^+$ and $Cl^-$ ions inside the membrane compared to the bulk fluid phase, which could partly account for their rejection. It was noted that $Cl^-$ ions experienced greater loss of their solvation shells compared to $Na^+$ ions, and $Cl^-$ exhibited preferential coordination with polymer hydroxyl hydrogen atoms, aromatic rings and amide hydrogen. Stronger coordination of the $Cl^-$ ion to polymer functional groups provided a plausible explanation for the reduced chloride mobility within the membrane compared to sodium. Using "umbrella sampling" for improved scanning of conformational space, and to determine the free energy of salt entrance into the membrane from the bulk aqueous phase, the researchers found significant, though variable, resistance for the entry of ions into the membrane interior. Gao et al. [30] similarly reported that $Na^+$ ions encountered a significant energy barrier for entry into a non-crosslinked PA model, but $Cl^-$ ions exhibited a slight attractive energy well proximal to the membrane interface. These observations stand in contrast to the findings of Luo et al. [38] described above, in which no entry barrier was detected using TMD simulations. Hughes and Gale [44] attributed ion-penetration resistance to charge separation near the membrane surface, resulting from differential disruption of the ion solvation shells as they approached and began to interact with the membrane matrix (Fig. 4). A similar mechanism was promulgated previously by Kotelyanskii et al. [26,33], but not explicitly derived. Hughes and Gale [44] suggested differential loss of ion hydration shells results in a variable effective dielectric constant whose magnitude depends on local water structure inside the membrane and its ability to reorganize to screen the Coulomb separation energy. The authors noted that the observed charge separation was consistent with an (*apparent*) absence of low-energy transmembrane pathways for coupled NaCl transport by an ion-pairing type of mechanism. However, it is worth emphasizing that this inference alone does not preclude existence of continuous ion-transport pathways transecting the membrane, similar to the meandering ion-transit pathways resolved by Luo et al. [38] using TMD simulations. Note that Shen and co-workers [32] also described what they referred to as "percolated free volume" pathways that continuously spanned their PA membrane models (see below).

Kolev and Freger [27,28] used a PA model building strategy conceptually similar to that originally described by Harder and co-workers [31], but instead employed different bond termination criteria based on atomic mass composition (C,O and N) and the fraction of residual (*i.e.,* non-crosslinked) carboxylate groups. The membrane model was hydrated by extended (100 ns) MD equilibration against a TIP3P water solution (0.6 g/cm$^3$) generating a chemical composition and degree of crosslinking (80.8%) in close agreement with recent experimental findings [45]. Radial distribution function (RDF) analyses of water inside the PA membranes were consistent with the presence of small network and large aggregate pores. However, the distribution of water around carboxylate groups was found to be unimodal and therefore could not be easily reconciled with an experimentally observed bimodal distribution of carboxylate p$K_a$ values previously reported by Coronell et al. [22]. Results from MD simulations up to 1000 ns in duration conducted by Kolev and Freger [28] suggested that water and solute permeation were mainly controlled by regions of high polymer density interspersed with more porous less dense domains. These authors also emphasized that ion adsorption was localized and depended to a large extent on heterogeneously-distributed partial atomic charges that effectively enhanced ion uptake while at the same time weakening salt exclusion due to fixed charges. A modified Donnan effect was invoked to explain ion sorption, but the authors did not discuss solvation/de-solvation effects that were shown in previous MD studies performed by Hughes and Gale [44] and

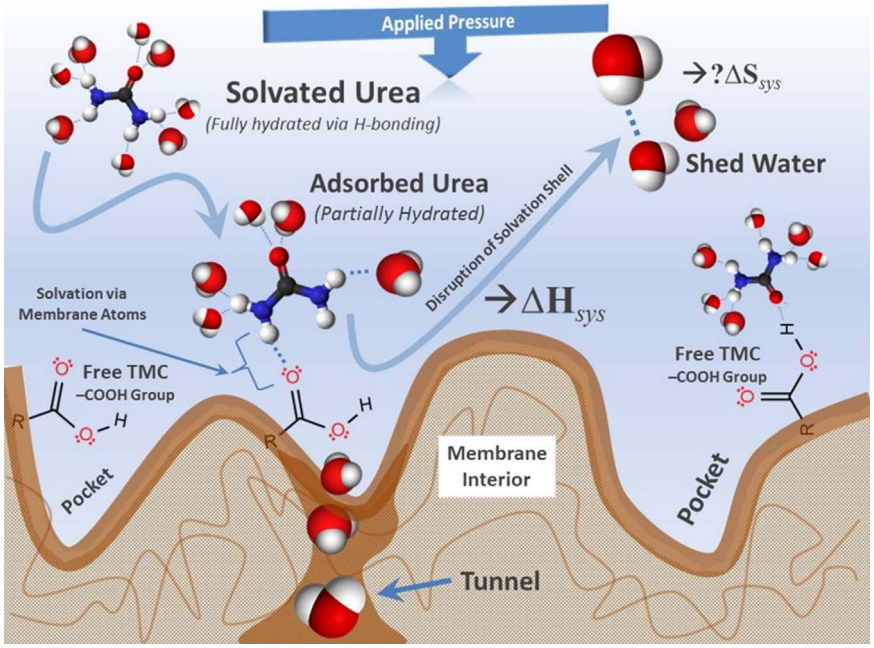



**Fig. 4.** Schematic illustrating the effects of shedding of solvation water in the adsorption of potential organic foulants to PA membranes. This basic mechanism, and variations of it, have been discussed in the publications of Hughes and Gale [58] and Shen et al. [48]. Here the rough membrane surface is represented by the thick wavy horizontal line (light brown), with the feed solution above the line (blue background) and the membrane network lying below (brown). Organic compounds having stronger (*i.e.,* tightly bound) hydration shells due to increased hydrogen-bonding interactions, such as urea (shown), are forced to shed waters of solvation at a larger thermodynamic penalty (→$\Delta H_{sys}$) compared to those with weaker shells as they approach and undergo binding to the membrane surface. The shed water molecules contribute to complex changes in the system entropy (→?$\Delta S_{sys}$), which presumably increases due to release from the organic solvation shell, but also decreases due to hydrogen-bonding interactions with the bulk water phase. (For interpretation of the references to color in this figure legend, the reader is referred to the web version of this article).

Luo et al. [38] to play important roles in ion access to the membrane surface and transport inside the membrane.

The structure and dynamics of water confined inside model PA membranes was recently explored by Ding and colleagues [39,40]. The authors built fully protonated (and ion-free) PA membrane models in a manner similar to that described by Hughes and Gale [44], in which a relaxed group of linear chains were first constructed followed by random crosslinking by a distance heuristic (see Fig. 3). The main advantage of such a build modality is that it allows the degree of crosslinking to be readily tuned so that structural and functional properties may be correlated with crosslink density. Water was modeled using a non-polarizable rigid TIP4P/2005 model [46] and was infused into the dry membrane by 10 ns of equilibrium MD against liquid reservoirs bracketing the membrane (NPT statistical ensemble). Membrane structure was characterized through local water density and cavity size distributions. Interactions between water molecules and the PA membrane were quantified by RDF methods. The simulations revealed that water preferentially interacted with oxygen and hydrogen atoms of the pendent carboxylic acid groups, as well as oxygen atoms of amide bonds. More than 90% of the embedded water molecules participated in contiguous hydrogen-bonded networks involving large clusters with about 575 members on average. This finding was comparable to that reported by Kotelyanskii et al. [26,33]; but in contrast to the Kotelyanskii studies, water diffusion inside the membrane was *not* characterized by sudden translational 'jumps' or 'hops'. On the other hand, large *rotational* displacements were observed for confined and bulk-phase water, even though overall rotary motions were significantly repressed inside the membrane. As reported in several prior simulations studies [26–28,33,44], the translational diffusion of confined water was reduced by about one order of magnitude compared to the bulk-phase (see Table 1), but only in the central part of the membrane. Weaker confinement effects in interfacial regions were correlated with an increased average cavity size close to the membrane/reservoir interfaces.

Gao et al. [30] recently described a fascinating previously unobserved effect in which water molecules inside PA membrane tunnels and pore spaces exhibited greatly accelerated pressure-driven (3 MPa; about 450 psi) translation (about 2.1 m/s) when the tunnel/pore dimensions were sufficiently small, typically less than about 30 Å in diameter on average. The researchers noted that under these conditions water-water intermolecular interactions were similar in magnitude to water-tunnel/pore interactions, which evidently promoted formation of water clusters, chains, or single-files that were attracted toward the tunnel walls. They coined the term "flush" diffusion to describe the anomaly and remarked this type of diffusion was much faster than the movement of water as a continuum through larger nanopores. The flush diffusion effect may be sufficiently dramatic as to classify it as a ballistic or super-diffusion regime. Similar kinetically-enhanced anomalous diffusion mechanics have been found *in silico* and experimentally demonstrated in carbon nanotubes and nanoporous graphene (see review by Thomas et al. [47]); and they do typically involve tunneling or porous transport and therefore may share comparable underlying mechanisms.

Finally, it should be added that the Gao PA membrane models were apparently not crosslinked, but instead consisted of a relaxed amorphous melt, which conceivably might have led to greater chain mobility than would be expected in a denser and fully crosslinked network [30]. The authors also reported significant compaction of their non-crosslinked PA models at pressures in excess of about 3 MPa, which resulted in water 'congestion' and reduced permeability.

Shen and co-workers [32,48] recently published a detailed account of PA membrane rejection mechanisms for NaCl and some small neutral organics, including methanol, ethanol, 2-propanol and urea. To build their PA membrane models, they employed a randomized solution bonding algorithm with a bond distance heuristic, essentially identical to that of Harder et al. [31]. However, unlike earlier studies, the authors employed non-equilibrium MD (NEMD) in which a pressure gradient (30–150 MPa) was applied across the model PA membranes. Pressure was introduced by applying differential forces to atoms in two graphene sheets bracketing the membrane system, thereby forcing water and solutes into the membrane. Perhaps not surprisingly, water transport was enhanced in membranes with larger solvent-accessible cavities. In addition, membranes swelled when hydrated, as noted in earlier modeling efforts [26–28,31,33]. The authors also reported their membranes vibrated due to molecular collisions allowing formation of contiguous but highly tortuous water (or solute) tunnels connecting opposite membrane faces, which is not unlike the trans-membrane TMD-resolved channels described by Luo et al. [38]. Solutes inside tunnels exhibited Brownian motion and 'hopped' from pore to pore as they transited the polymer network [32]. A significant finding was that a non-monotonic relationship was observed between rejection and ion (or solute) size. For example, $Na^+$ with a comparatively small VDW radius of about 1.4 Å was rejected better than urea (2.4 Å radius) or ethanol (2.6 Å radius) with larger radii [32]. Higher rejection for smaller solutes was reconciled by showing ion-water pair potentials were > 2x stronger than the hydrogen-bond energy for organic solutes, suggesting the hydration shell controls rejection by invoking a thermodynamic penalty for shedding one or more water molecules from shells during membrane transport (see Fig. 4, above). Thus, although urea and ethanol are comparable in size, the former exhibits more hydrogen bonding than ethanol leading to a higher rejection. This finding is conceptually similar to that set forth by Hughes and Gale [44] regarding entrance of $Na^+$ and $Cl^-$ ions into their PA membranes. Presumably, fully hydrated ions or organics larger than membrane nanopores require shedding proportionately more solvation waters to enter and transit the pore and tunnel networks. Shen and colleagues [32] also point out that the ion-solvent interaction is less sensitive to orientation than hydrogen bond interactions, making ion-water pairing generally more thermodynamically stable than organic-water pairing.

In recent years there has been considerable interest in the design, evaluation and commercialization of hybrid nanoparticle-polyamide (*i.e.*, nanocomposite) membranes using a variety of nanoparticle types, including zeolites and carbon nanotubes (CNTs) [49,50]. In one recent publication, Araki and co-workers [51] describe MD simulations of a mixed PA-CNT membrane material. These authors were particularly interested in how the presence of single-wall CNTs embedded in the PA matrix influenced molecular structure and transport properties compared to conventional PA models devoid of CNTs. A comparatively fast water diffusion rate of $3.38 \times 10^{-9}$ $m^2/s$ was averaged over their model membranes (see Table 1, above). It was found that the addition of CNTs diminished the mean pore size of the composite membrane and increased rejection of $Na^+$ and $Cl^-$ ions. Statistical-mechanical analyses using RDF methods revealed that water confined in the pore spaces of the nanocomposite membranes exhibited smaller clusters, which was consistent with a somewhat denser membrane structure (nanocomposite membranes were about 3.9% denser than unadulterated PA membranes). The researchers also described a statistically favored formation of small polymer ring structures containing 4-6 MPD-TMC residues in some of their models, presumably due to self-crosslinking between closely located reactive groups.

It a recent related (nanocomposite) modeling effort, Liyana-Arachchi et al. [52] reported use of a "molecular-layer-by-layer" (mLbL) approach to build PA membranes on top of a silicon wafer. The mLbL procedure and force field models used were validated by comparison with available experimental data with respect to hydrated density, membrane swelling, thickness, degree of crosslinking, and pore size distributions. Fully atomistic MD simulations showed that mLbL deposition produced membranes at a constant film growth if the MPD/TMC monomer ratio was constant. It was also reported that both TMC and MPD oriented at a tilted angle with respect to the silicon wafer substrate and that the angular distribution depended on the TMC

growth rate and number of deposition cycles.

## 3. Molecular simulations of foulant adsorption onto polyamide membrane materials

The most critical problem currently limiting the performance of the current generation of permselective PA (and other) membrane materials for desalination and reuse is the irreversible adsorption of natural organic matter (NOM) and microorganisms (in the form of biofilms) to membrane surfaces. Both NOM and biofouling processes degrade membrane energy efficiency by obstructing access of water to the membrane surface, thereby leading to loss of water flux [53–55]. Moreover, biofouling in particular can amplify concentration polarization effects within the water-membrane interfacial region through the buildup of a biological hydrogel at the feed surface, resulting in a counterproductive osmotic gradient that decreases the effective applied pressure leading to flux and rejection losses [56,57]. Because of these issues, understanding how bio-organic molecules undergo adsorption to membrane materials has direct implications for lowering desalination energy costs in the future, extending membrane and facility lifetimes, and improving cleaning methods.

Molecular modeling of foulant-membrane adsorption processes has recently begun to shed light on the nature and diversity of mechanisms involved in bio-organic fouling of RO and other membrane materials. For example, Hughes and Gale [58] reported the use of MD simulations to explore how certain small organic and inorganic compounds, including glucose, phenol and $O_2$ gas, interact with RO membrane surfaces to cause fouling. Glucose and phenol were selected since they represent two of the basic building blocks of NOM. Results of unbiased MD simulations and umbrella-sampling methods showed each of the three foulants interacted with the membrane in a different manner; and that the organics bound more strongly to the membrane than $O_2$. Glucose diffused onto the surface of the membrane and entered into multiple H-bonds with polymer functional groups. Phenol not only adsorbed to the membrane surface, but in some cases diffused through membrane pores, possibly as a result of its more hydrophobic nature. The presence of both organic foulants on the membrane surface reduced the rate of exchange of water molecules across the membrane interface, suggesting they could cause flux decline in actual membrane systems. The authors also observed (in umbrella sampling runs) structural rearrangements of the membrane that were potentially correlated with the binding and release of the foulant molecules.

As alluded to in the previous section, Shen and co-workers [48] using an NEMD protocol drove various organic compounds (methanol, ethanol, 2-propanol and urea) into their PA membrane models under an applied pressure. The initial adsorption of the organics onto the membrane surface and their subsequent passage across the membrane interior was correlated to how strongly each compound was solvated. Organic compounds having stronger (*i.e.,* more tightly bound) hydration shells (*e.g.,* through hydrogen bonding) are forced to shed waters of solvation at a larger thermodynamic penalty compared to those with weaker shells as they approach and bind to the membrane surface. Thus, water shell structure and the degree of solvation shell disruption appear to play important roles in determining whether foulant adsorption is thermodynamically favorable (see Fig. 4, above). Along the same lines, it would be interesting to also quantify how the disruption of membrane solvation shells by approaching foulant molecules influences foulant binding and behavior.

It should be stressed here that the concept of solvation-desolvation, often used to describe the thermodynamic state of ions or polar molecules in aqueous media, or its change upon transfer between different media, is addressed in a natural way in MD simulations, *i.e.*, solvation energy is obtained directly, without invoking any *ad hoc* assumptions of a solvation sheath.

In two recent related publications, Xiang et al. [41,42] describe the application of "steered" MD (SMD) simulations to determine how non-acetylated (algal) alginate undergoes binding to PA membrane surfaces. In the SMD protocol used, alginate was first permitted to adsorb to the solvated PA membrane surface, after which it was gradually "pulled" away from the surface to measure the thermodynamic binding energy. The force curves generated typically exhibited multiple peaks corresponding to distinct binding events or mechanisms (*e.g.,* ion bridging *versus* H-bonding or VDW interactions). Results from both reports indicated carboxylate groups located at the PA surface and on alginate chains exhibited strong binding with metal ions, specifically $Na^+$ and $Ca^{2+}$. While both cations mediated alginate adsorption to the PA models, $Ca^{2+}$ ions interacted more strongly with free carboxylate groups and were found to promote alginate binding by mono- and bidentate ionic bridging mechanisms. Interestingly, Ahn et al. [58] did not observe cationic ($Ca^{2+}$ or $Mg^{2+}$) bridging in their MD simulations of NOM adsorption to a polyethersulfone (PES) membrane model, presumably because the NOM carboxyl groups associated with the divalent ions, but the PES sulfonyl groups did not.

Of particular interest in the Xiang study [42] was the observation that the "binding breakdown time" (*i.e.*, the time needed to reach a precipitous decline in binding energy in the SMD simulations) was shorter for $Ca^{2+}$ than $Na^+$ ions, presumably because of a higher solvation free energy for $Ca^{2+}$ ions. When multiple alginate oligomers were introduced (as a surrogate hydrogel), they too adsorbed to the PA surface forming a web-like structure [42]. The authors described two interesting phenomena for the alginate hydrogel model, including (1) clear involvement of short-range hydrogen bonding and VDW attraction forces in stabilizing gel adhesion, and (2) stretching type deformations of the alginate and PA chains as manifested by longer pulling distances.

Recent experimental findings suggest the existence of multiple membrane fouling mechanisms as the diversity and complexity of the foulant species increases and molecular simulations have begun to play a role in elucidating how foulant mixtures interact with membrane surfaces. For example, Myat and co-workers [60] demonstrated complexion between BSA-humic and alginate-humic substances leading to aggregation and reversible cake formation on polypropylene MF membranes. Fouling for the BSA-humic mixture was greater than fouling of the individual solutions. In contrast, the fouling rate for the $Na^+$-alginate-humic mixture was similar to that of $Na^+$-alginate alone. Molecular dynamics simulations were consistent with the experimental observations and further indicated alginate-humic interactions were arbitrated by water-mediated cation bridging between deprotonated carboxylate groups on the humic acid molecule and a binding pocket on the alginate. The BSA-humic interactions, on the other hand, were driven mainly by hydrogen-bonding and hydrophobic interactions, but were largely unaffected by $Ca^{2+}$ ions. The hydrophobic interactions involved a proline residue on the protein surface and aromatic rings associated with the humic acid.

More recently, Xiang and co-workers [43] employed SMD simulations to investigate the interaction of alginate with a polyethylene glycol (PEG)-grafted PA membrane surface. The objective in this study was to determine if the highly hydrophilic PEG layer could weaken alginate adsorption, thereby serving as an anti-fouling coating. The authors noted that the alginate gel encountered a strong repulsive force as it was "dragged" toward the PEG-coated surface, evidently due to compression of the PEG solvation layer. One interesting observation was that the alginate gel exhibited a strong tendency to drift off axis toward areas of the PA membrane where the PEG coating was thinnest or absent (referred to as "PEG hollows"). The findings reported are consistent with the hypothesis that PEG could serve as an effective anti-fouling modality.

## 4. Modeling issues and concerns

Several issues remain concerning molecular modeling of RO and related membrane materials. One concern is that the demonstrated

physicochemical heterogeneity of PA membranes in terms of polymer distribution, thickness, ionization state, and surface roughness make it difficult to know what features of the membrane to model (see Fig. 2). For example, in the majority of MD simulations studies, care was taken to thermodynamically relax the PA models over many tens or hundreds of ns, sometimes at temperatures exceeding 1000 °K. Yet, the interfacial polymerization reaction used to synthesize PA thin films is one of the fastest reactions known [61,62]. Indeed, interfacial polymerization with MPD and TMC is so rapid under ideal conditions that the densified membrane polymer networks produced may never come to true equilibrium, but instead quickly gel (*via* "rigid" crosslinks) into an inhomogeneous and thermodynamically unstable configuration. Yet, as modelers of such materials, it is usually assumed that the actual membranes exist in a completely relaxed state at a given temperature-pressure ensemble. But this presupposition may or may not be true; and it would therefore be instructive to prepare PA models spanning a range of conformational states that vary from extremely strained to largely unstrained configurations to determine their unique architectural differences that ultimately determine cavity-size/shape distributions, transport properties, and surface-fouling behaviors.

As previously mentioned, while some researchers have chosen to build their PA membrane models by fully protonating non-crosslinked (free) carboxyl groups (-R-COOH), others have left these groups in the ionized carboxylate form (-R-COO-), which is the form they would normally adopt when exposed to actual feedwaters. While this difference may appear to be of little concern to some, it could lead to subtle changes in the magnitude and distribution of atomic partial charges over the membrane model. With the possible exception of the work reported by Kolev and Freger [27], there have so far been no rigorous comparisons made between the properties of fully protonated *versus* non-protonated PA models, or the influence of the counterion type. Indeed, Kolev and Freger [27] reported significant differences between the two membrane forms regarding the scalar self-diffusion velocities of SPC water models and $Na^+$ ions embedded in the membrane (larger rates for the neutral membrane, despite greater hydration). Given this result, it is reasonable to speculate that subtle alterations in atomic partial charges might lead to significant cumulative effects in terms of chain interactions, hydrogen bonding and folding, which in turn could influence performance.

Huges and Gale [44] expressed concern over uncertainty about the effective dielectric constant associated with partially solvated ions at the membrane surface or inside the membrane. The authors reported that when efforts were made to separately force a $Na^+$ or $Cl^-$ ion into the membrane, an increasing free-energy profile was recorded to a depth of 10 Å or more. They reasoned this behavior resulted from increasing Coulomb separation energy of the ion pair combined with a variable effective dielectric constant that would be dependent on the local water structure in the membrane and its ability to reorient to occlude the electrostatic interaction.

Questions may also be posed about the way in which the PA models are constructed by various researchers. For example, does a reactive MPD + TMC "soup" with progressive crosslinking best emulate actual PA membrane synthesis? Models built in this manner tend to suffer from rapid depletion of MPD residues as polymerization proceeds, thereby requiring periodic replenishment of this residue to drive crosslinking toward completion. Yet, such replenishment typically does not occur in practice and real PA films terminate their growth as chemically asymmetric structures [cf., 15]. Perhaps future modeling protocols should take such asymmetry into account, or at least try to better mimic the specific compositional details that describe the feed surfaces, such as the possibility of reduced crosslinking, more total charge, density differences, higher TMC density, *etc.*

Other modeling observations defy clear understanding at this juncture. For example, a mechanistic explanation for the accelerated transit of water molecules through relatively narrow PA tunnels, termed 'flush' diffusion by Gao et al. [30], remains nebulous. Whether flush diffusion shares underlying physiognomies with similar rapid water diffusion processes, such as those observed in single-wall CNTs [46], is still unknown, but both phenomena involve tunnel-induced transport where wall interactions are important. It will be interesting to learn if other researchers will be able to reproduce this anomalous diffusion regime using different MD algorithms and water models.

Xiang and colleagues [42,43] made the intriguing observation that when adsorbed alginate was pulled away from the PA membrane interface using SMD, the PA chains experienced local distortion and stretching. It therefore seems plausible that biofoulant adsorption may be able to modify the membrane surface, possibly irreversibly, which in turn might influence how water and solutes interact with the membrane. It is not unreasonable to postulate that other types of organic foulants, such as polypeptides, phospholipids, NOM, nucleic acids, and other biological macromolecules known to be problematic in actual RO systems, would lead to even more severe molecular-level changes to the PA surface. A corollary question is: Does such organic foulant adsorption substantially affect water adsorption and penetration into pressurized membranes, *i.e.*, how is flux affected, if at all? These and related questions will likely be addressed in future modeling programs.

An important issue in MD simulations of foulant (or solute) adsorption is selection of the area on the membrane model surface where a ligand will be initially placed to study its binding behavior. As mentioned in previous sections of this review, the PA membrane surface is highly irregular and comprised of hollow protuberances and valleys at both the atomic and nanoscales. Because of this irregular topology, it is easy to imagine that there might be adsorption "hot-spots" or "pockets", such as molecular valleys, where foulant molecules (ligands) would have a greater opportunity to interact with membrane atoms *via* hydrogen bonding and solvation mechanisms and undergo strong binding.

In the majority of MD studies of ligand-membrane binding, this potential topological influence has not been adequately addressed. Instead, a ligand is most often simply placed near the central region of a membrane model and allowed to undergo adsorption (*via* MD) at that particular locus. However, such a protocol may or may not yield a low-energy binding potential depending on the choice of the initial ligand location above the membrane surface. For example, Hughes and Gale [58] noted that glucose molecules introduced above their model PA membrane surfaces underwent initial binding to the membrane, but then in extended (6 ns) MD simulations detached and later reattached multiple times at various membrane locations. Xiang et al. [41] accounted for this kind of effect by first performing a series of short preliminary MD binding simulations at a number of different membrane loci, then choosing the locus that had yielded the strongest initial binding to carry out an extended MD simulation.

The concept of ligand binding to a morphologically heterogeneous membrane surface exhibiting molecular-scale "hills and valleys", as well as deeper nanopores, is illustrated in Fig. 5. To better negotiate a complex (uneven) membrane topology, an initial rapid screening protocol can be employed to provide an approximation of ligand binding strength at many different surface loci. One possible screening approach, which is outlined in Fig. 6, introduces the ligand in a random or systematic manner over many different membrane loci. At each location, the flexible ligand is allowed to search phase-space for the lowest-energy bound configuration, which can be done with a minimum of computational cost by a series of geometry optimizations alternated with Monte-Carlo-like moves. Of the many ligand configurations offered to the membrane at a particular locus, the one with the lowest (strongest) interaction energy with the membrane is recorded and subsequently used for comparison with alternative loci. The membrane locus exhibiting the strongest interaction.

potential can then be selected for more detailed MD studies. This general approach is somewhat analogous to that employed in "virtual ligand screening" (VLS) assays in pharmacological drug-discovery

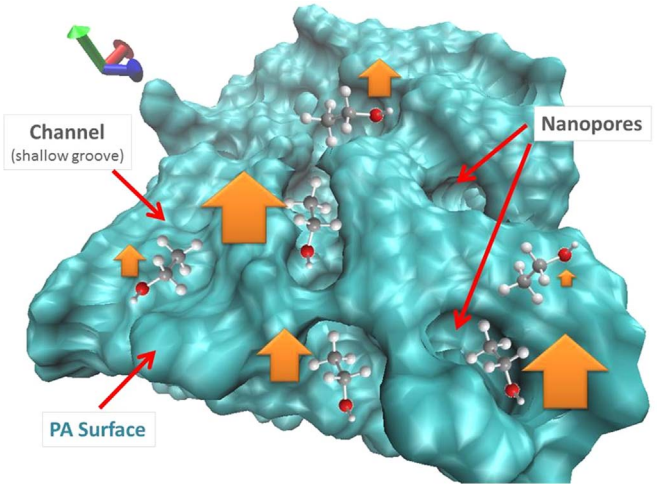



**Fig. 5.** Concept of ligand (solute or foulant) binding to a morphologically heterogeneous PA membrane surface exhibiting an uneven landscape. See text for details. The hypothetical PA surface is rendered as a Connolly probe surface (probe diameter=1.4 Å). Small ligands or foulant molecules, such as ethanol shown in this instance, may undergo strong or weak binding depending on where adsorption takes place. Adsorption within deep nanopores or grooves have the potential to strengthen binding by maximizing the number of attractive intermolecular interactions. In the diagram, strong ethanol binding is illustrated by the larger orange-colored arrows; weaker binding by smaller arrows.

studies, in which the binding strength of a ligand (potential drug candidate) is calculated for different conformational "poses" within the active sites of target enzyme or receptor molecules [63–65]. Drug candidates displaying strong binding characteristics are selected as potential lead compounds.

## 5. Concluding remarks and future prospects

Two key technological challenges for the desalination and water-reuse communities are: (1) organic and biological fouling of RO and NF membrane surfaces leading to deterioration of energy performance and lifetime, and (2) concern over the rejection of *specific* trace organic compounds that are deleterious to human health and/or the environment. This review has provided an overview of the current status of molecular simulations of PA membrane materials and how modeling at the atomic scale can help resolve and elucidate fundamental transport and fouling mechanisms. The studies cited in this review suggest that classical equilibrium MD simulations and related non-equilibrium approaches (*e.g.*, SMD, TMD) can be extremely valuable for not only probing membrane structure and function at scales not typically accessible by most surface analytical techniques, but also for empowering the design of the next generation of RO membranes.

Although significant differences were observed across the various membrane modeling studies, there is also surprising agreement. Most studies employed different force fields and parameters (*e.g.*, OPLSS-AA, AMBER, CVFF, *etc.*), as well as different commercial and open-source MD engines and integration algorithms (*e.g.*, DLPOLY, LAMMPS, NAMD, GROMACS, *etc.*). Other differences included the use custom membrane-building algorithms (*e.g.*, amorphous melts *versus* crosslinked networks), different water models (*e.g.*, TIP3P, SPC, TIP4P, CVFF, *etc.*) and different model equilibration and optimization times ranging from a few hundred ps in earlier studies to > 1000 ns in later investigations (see Table 1, above).

In spite of such technical disparities, common membrane attributes are evident across the different modeling studies making it possible to construct a somewhat generalized image incorporating the salient features of these functional materials. For example, one nearly universal theme, first introduced by Kotleyanskii et al. [26,33] and later expanded in the reports by Hughes and Gale [44] and Shen and co-workers [32], is the importance of interfacial water structuring and solvation/de-solvation effects in facilitating (or in some cases retarding) inorganic solute and/or organic foulant association with and transport within PA membranes.

A particularly encouraging point is that, regardless of the particular PA model used, strikingly similar values for water permeability have been reported (see Table 1, above), which lends considerable credence to the MD estimates. A similar table for salt and ion permeability, for which data are more scarce, might be expected to yield less consistent results, possibly because ion permeation is more sensitive to the detailed atomic and nanoscale assembly of membranes, a relationship that should be more closely examined in future MD efforts. Furthermore, it is unclear if the simulations that have been conducted

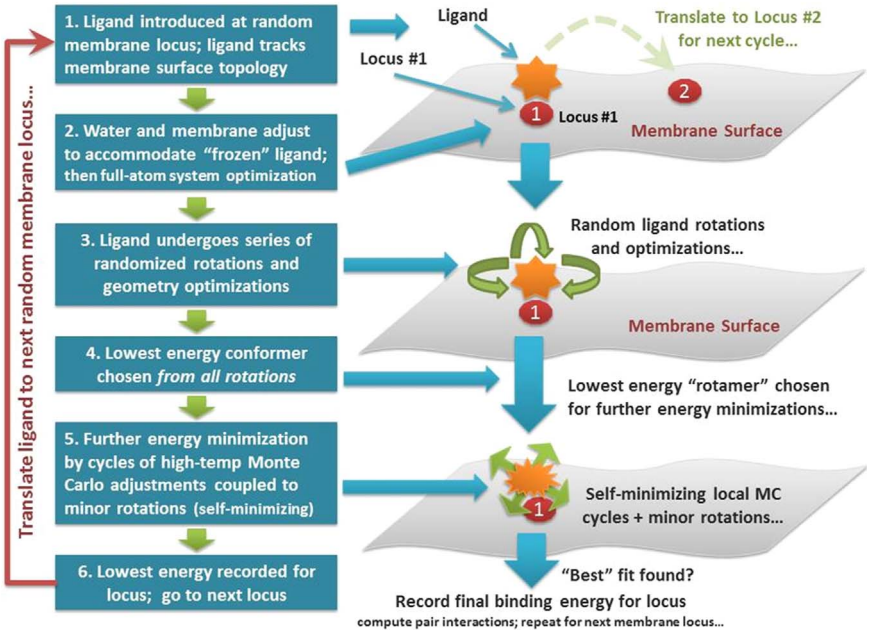



**Fig. 6.** Flow schematic of possible steps in a rapid screening protocol to compute approximate ligand (foulant) binding strengths at different PA membrane loci. Implementing such an approach can be used to identify ligand-binding "hotspots". See text for details.

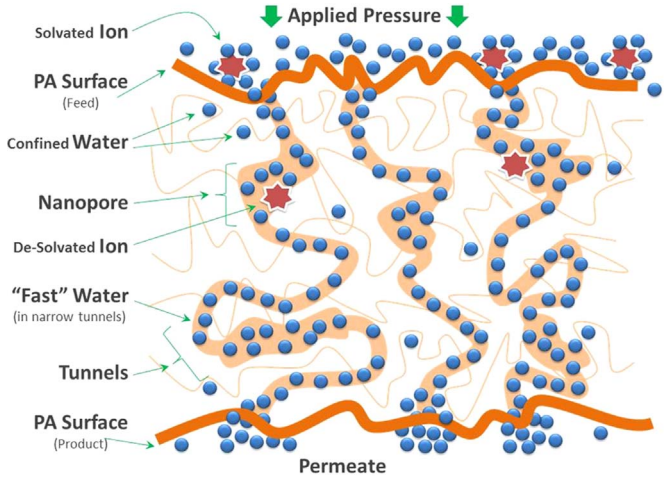



**Fig. 7.** Schematic summarizing some of the key features of semipermeable PA membrane materials that have emerged from molecular modeling studies in recent years. The membrane is a dynamic polymer network that continually vibrates and alters its conformation around some "ergodic" or time-average structure. Thus, although they are quasi-stable, transmembrane tunnels and nanoporous regions can form and decay depending on local solvation and ion interactions. Depending on tunnel dimensions and composition, water molecules placed under a driving pressure may exhibit anomalous "fast" transport kinetics, referred to by Gao and co-workers [30] as "flush" diffusion. Extensively hydrogen-bonded "continuum" or clustered water, resembling that of bulk water in terms of its density and diffusion properties, primarily exists inside the membrane in expanded nanopores. Both water and solutes appear to transit the membrane *via* a jump or hopping mechanism in which the frequency of jumps controls the water production rate (*i.e.*, membrane flux).

to date have been of sufficient duration to fully capture the permeation characteristics of solute transport.

Based on the simulations reviewed, RO membranes can be envisioned as vibrant dynamic polymer networks comprised of tangled and highly crosslinked PA chains pervaded by tortuous, water-filled transmembrane tunnels (channels) of continually varying dimensions that facilitate pressure-driven water transport and solute rejection (see Fig. 7). The tunnels should not be thought of as rigid permanent structures with fixed diameters and lengths, but rather they continually undergo localized (thermodynamically-mediated) flexion, swelling and contraction leading to the transient existence of not only tunneling bottlenecks, but also expanded nanoporous regions containing continuous hydrogen-bonded water complexes (so-called 'continuum' water). It is also clear from the computational studies that the PA surfaces are quite rough on a molecular scale with a diffuse ill-defined boundary shared with the liquid phase [32,48]. Furthermore, the polymer density and conformational space of the PA chains rapidly respond to local shifts in water activity, as well as the type and concentration of ions present. These dynamic fluctuations result in a kind of time-averaged "ergodic" structure that,

when exposed to a differential pressure, leads to preferential solute rejection and enhanced water flow through the tunneling network.

Despite this highly generalized picture, many questions remain concerning the details of membrane structure and function, particularly regarding the exact role of solvation and hydrogen-bonding energetics with respect to water and ion entrance into a membrane polymer that is significantly dehydrated compared to the bulk aqueous phase. For example, there appear to be few if any reliable estimates comparing the thermodynamics of sequential shedding of solvation waters with entropic increases experienced inside the membrane when an ion (or water molecule) undergoes re-solvation by one or more membrane atoms. Such calculations may require the challenging task of modeling much smaller regions of membrane over greater phase-space using appropriate quantum-level methods.

Future modeling efforts will likely be increasingly directed toward deciphering how specific trace organic compounds that have public health significance will interact with conventional and chemically modified PA membranes and undergo rejection or transport. Given the very large chemical diversity of such compounds (including disinfection byproducts, endocrine disruptors, personal care products, *etc.*), it seems probable that many novel transport/rejection pathways will be discovered, particularly as modeling theory and protocols continue to evolve and improve over the coming years.

## References

[1] C.E. Reid, E.J. Breton, Water and ion flow across cellulosic membranes, J. Appl. Polym. Sci. 1 (1959) 133–143.
[2] C.E. Reid, J.R. Kuppers, Physical characteristics of osmotic membranes of organic polymers, J. Appl. Polym. Sci. XX (1959) 264–272.
[3] S. Loeb, The Loeb-sourirajan Membrane: How It Came About in Synthetic Membranes 153, American Chemical Society, Washington, DC, 1981, pp. 1–9.
[4] J. Glater, The early history of reverse osmosis membrane development, Desalination 117 (1998) 297–309.
[5] R.L. Riley, J.O. Gardner, U. Merten, Cellulose acetate membranes: electron microscopy of structure, Science 143 (1964) 801–803.
[6] P.H. Carnell, H.G. Cassidy, The preparation of membranes, J. Polym. Sci. 55 (1961) 233–249.
[7] L.T. Rozelle, J.E. Cadotte, R.D. Corneliussen, E.E. Erickson, Development of New Reverse Osmosis Membranes for Desalination, Report No. PB-206329, Spring-Reld, IL: VA National Technical Information Service, 1967.
[8] J.E. Cadotte, Reverse Osmosis Membrane, U.S. Patent 4,039,440, 2 August 1977.
[9] J.E. Cadotte, R.J. Petersen, R.E. Larson, E.E. Erickson, A new thin-film composite seawater reverse osmosis membrane, Desalination 32 (1980) 25–31.
[10] U. Merten, Flow relationships in reverse osmosis, Ind. Eng. Chem. Fundam. 2 (1963) 229–232.
[11] H.K. Lonsdale, U. Merten, R.L. Riley, Transport properties of cellulose acetate osmotic membranes, J. Appl. Polym. Sci. 9 (1965) 1341–1362.
[12] D.R. Paul, Reformulation of the solution-diffusion theory of reverse osmosis, J. Membr. Sci. 241 (2004) 371–386.
[13] K. Merrett, R.M. Cornelius, W.G. McClung, L.D. Unsworth, H. Sheardown, Surface analysis methods for characterizing polymeric biomaterials, J. Biomater. Sci. Polym. 13 (2002) 593–621.
[14] L. Lin, R. Lopez, G.Z. Ramon, O. Coronell, Investigating the void structure of the polyamide active layers of thin-film composite membranes, J. Membr. Sci. 497 (2016) 365–376.
[15] F. Pacheco, R. Sougrat, M. Reinhard, J.O. Leckie, I. Pinnau, 3D visualization of the internal nanostructure of polyamide thin films in RO membranes, J. Membr. Sci. 501 (2016) 33–44.
[16] F.A. Pacheco, Microscopic Characterization of the Nanostructure of Polyamide Thin Films in Reverse Osmosis and Nanofiltration Membranes PhD Dissertation, Stanford University, USA, 2011.
[17] T.D. Matthews, H. Yan, D.G. Cahill, O. Coronell, B.J. Mariñas, Growth dynamics of interfacially polymerized polyamide layers by diffuse reflectance spectroscopy and Rutherford backscattering spectrometry, J. Membr. Sci. 429 (2013) 71–80.
[18] S. Karan, Z. Jiang, A.G. Livingston, Sub–10 nm polyamide nanofilms with ultrafast solvent transport for molecular separation, Sci. Mag. 348 (2015) 1347–1351.
[19] T. Fujioka, N. Oshima, R. Suzuki, W.E. Price, L.D. Nghiem, Probing the internal structure of reverse osmosis membranes by positron annihilation spectroscopy: gaining more insight into the transport of water and small solutes, J. Membr. Sci 486 (2015) 106–118.
[20] O. Coronell, B.J. Marinas, D.G. Cahill, Depth heterogeneity of fully aromatic polyamide active layers in reverse osmosis and nanofiltration membranes, Environ. Sci. Technol. 45 (2011) 4513–4520.
[21] O. Coronell, B.J. Mariñas, X. Zhang, D.G. Cahill, Quantification of functional groups and modeling of their ionization behavior in the active layer of FT30 reverse osmosis membrane, Environ. Sci. Technol. 42 (2008) 5260–5266.
[22] O. Coronell, M.I. González, B.J. Mariñas, D.G. Cahill, Ionization behavior, stoichiometry of association and accessibility of functional groups in the active layers of reverse osmosis and nanofiltration membranes, Environ. Sci. Technol. 44 (2010) 6808–6814.
[23] H.F. Ridgway, J.D. Gale, Z.E. Hughes, M.B. Stewart, J.D. Orbell, S.R. Gray, Molecular scale modeling of membrane water treatment processes, in: M. Duke, D. Zhao, R. Semiat (Eds.), Functional Nanostructured Materials and Membranes for Water Treatment (Nanomaterials for Water), Elsevior Publishing, New York, 2013, pp. 249–299.
[24] H. Elbro, Y.M. Kim, J.H. Kim, Molecular dynamics simulations in membrane-based water treatment processes: a systematic overview, J. Mem. Sci 438 (2013) 112–125.
[25] R. Oizerovich-Honig, V. Raim, S. Srebnik, Simulation of thin film membranes formed by interfacial polymerization, Langmuir 26 (2010) 299–306.
[26] M.J. Kotelyanskii, N.J. Wagner, M.E. Paulaitis, Atomistic simulation of water and salt transport in the reverse osmosis membrane FT-30, J. Membr. Sci 139 (1998) 1–16.
[27] V. Kolev, V. Freger, Hydration, porosity and water dynamics in the polyamide layer of reverse osmosis membranes: a molecular dynamics study, Polymer 55 (2014) 1420–1426.
[28] V. Kolev, V. Freger, Molecular dynamics investigation of ion sorption and permeation in desalination membranes, Phys. Chem. B 119 (2015) 14168–14179.

[29] L. Masaro, X.X. Zhu, Physical models of diffusion for polymer solutions, gels and solids, Prog. Polym. Sci. 24 (1999) 731–775.
[30] W. Gao, F. She, J. Zhang, L. Dumée, L. He, P.D. Hodgson, L. Kong, Understanding water and ion transport behavior and permeability through poly(amide) thin film composite membrane, J. Membr. Sci 487 (2015) 32–39.
[31] E. Harder, D.E. Walters, Y.D. Bodnar, R.S. Faibish, B. Roux, Molecular dynamics study of a polymeric reverse osmosis membrane, J. Phys. Chem. B 113 (2009) 10177–10182.
[32] M. Shen, S. Keten, R.M. Lueptow, Dynamics of water and solute transport in polymeric reverse osmosis membranes via molecular dynamics simulations, J. Membr. Sci. 506 (2016) 95–108.
[33] M.J. Kotelyanskii, N.J. Wagner, M.E. Paulaitis, Molecular dynamics simulation study of the mechanisms of water diffusion in a hydrated, amorphous polyamide, Comput. Theor. Polym. Sci. 9 (1999) 301–306.
[34] S. Riniker, J.R. Allison, W.F. vanGunsteren, On developing coarse-grained models for biomolecular simulation: a review, Phys. Chem. Chem. Phys. 14 (2012) 12423–12430.
[35] P. Meakin, I. Majid, S. Havlin, H.E. Stanley, Topological properties of diffusion limited aggregation and cluster-cluster aggregation, J. Phys. A: Math. Gen. 17 (1984) L975–L981.
[36] M.C.Y. Wong, L. Lin, O. Coronell, E.M.V. Hoek, G. Ramon, Impact of liquid-filled voids within the active layer on transport through thin-film composite membranes, J. Membr. Sci 500 (2016) 124–135.
[37] A.-H.M.A. El-Aassar, Polyamide thin film composite membranes using interfacial polymerization: synthesis, characterization and reverse osmosis performance for water desalination, Aus. J. Basic Appl. Sci 6 (2012) 382–391.
[38] Y. Luo, E. Harder, R.S. Faibish, B. Roux, Computer simulations of water flux and salt permeability of the reverse osmosis FT-30 aromatic polyamide membrane, J. Membr. Sci 384 (2011) 1–9.
[39] M. Ding, A. Szymczyk, F. Goujon, A. Soldera, A. Ghoufi, Structure and dynamics of water confined in a polyamide reverse-osmosis membrane: a molecular-simulation study, J. Membr. Sci 458 (2014) 236–244.
[40] M. Ding, Molecular Simulations of Reverse Osmosis Membranes Ph.D. thesis, Institut des Sciences Chimiques de Rennes, Composante universitaire SPM, Paris, France, 2015.
[41] Y. Xiang, Y. Liu, B. Mi, Y. Leng, Hydrated polyamide membrane and its interaction with alginate: a molecular dynamics study, Langmuir 29 (2013) 11600–11608.
[42] Y. Xiang, Y. Liu, B. Mi, Y. Leng, Molecular dynamics simulations of polyamide membrane, calcium alginate gel, and their interactions in aqueous solution, Langmuir 30 (2014) 9098–9106.
[43] Y. Xiang, R.-G. Xu, Y. Leng, Molecular dynamics simulations of a poly(ethylene glycol)-grafted polyamide membrane and Its interaction with a calcium alginate gel, Langmuir 32 (2016) 4424–4433.
[44] Z.E. Hughes, J.D. Gale, A computational investigation of the properties of a reverse osmosis membrane, J. Mater. Chem. 20 (2010) 7788–7799.
[45] X. Zhang, D.G. Cahill, O. Coronell, B.J. Marinas, Absorption of water in the active layer of reverse osmosis membranes, J. Membr. Sci. 331 (2009) 143–151.
[46] H.W. Horn, W.C. Swope, J.W. Pitera, J.D. Madura, T.J. Dick, G.L. Hura, T. Head-Gordon, Development of an improved four-site water model for biomolecular simulations: TIP4P-Ew, J. Chem. Phys. 120 (2004) 9665.
[47] M. Thomas, B. Corry, T.A. Hilder, What have we learnt about the mechanisms of rapid water transport, ion rejection and selectivity in nanopores from molecular simulation?, Small 10 (2014) 1453–1465.
[48] M. Shen, S. Keten, R.M. Lueptow, Rejection mechanisms for contaminants in polymeric reverse osmosis membranes, J. Membr. Sci. 509 (2016) 36–47.
[49] W.J. Lau, S. Gray, T. Matsuura, D. Emadzadeh, J.P. Chen, A.F. Ismail, A review on polyamide thin film nanocomposite (TFN) membranes: History, applications, challenges and approaches, Water Res. 80 (2015) 306–324.
[50] B.-Y. Jeong, E.M.V. Hoek, Y. Yan, A. Subramani, X. Huang, G. Hurwitz, A.K. Ghosh, A. Jawor, Interfacial polymerization of thin film nanocomposites: a new concept for reverse osmosis membranes, J. Membr. Sci 294 (2007) 1–7.
[51] T. Araki, R. Cruz-Silva, S. Tejima, K. Takeuchi, T. Hayashi, S. Inukai, T. Noguchi, A. Takeuchi, T. Kawaguchi, M. Terrones, M. Endo, Molecular dynamics study of carbon nanotubes/polyamide reverse osmosis membranes: polymerization, structure, and hydration, ACS Appl. Mater. Interfaces 7 (2015) 24566–24575.
[52] T.P. Liyana-Arachchi, J.F. Sturnfield, C.M. Colina, Ultrathin molecular-layer-by-layer polyamide membranes: insights from atomistic molecular simulations, J. Phys. Chem. B (2016) Article ASAP.
[53] M.T. Khan, Fouling of Seawater Reverse Osmosis (SWRO) Membrane: Chemical and Microbiological Characterization (Ph.D. Dissertation), King Abdullah University of Science and Technology, Saudi Arabia, 2013.
[54] N. Pena, S. Gallego, F.del Vigoa, S.P. Chesters, Evaluating impact of fouling on reverse osmosis membranes performance. in: Proceedings of the International Conference on Desalination for the Environment, Clean Water and Energy, European Desalination Society, Barcelona, Spain, 23–26 April 2012.
[55] H.F. Ridgway, H.-C. Flemming, Membrane biofouling, in: J. Mallevialle, P.E. Odendaal, M.R. Weisner (Eds.), Water Treatment: Membrane Processes, McGraw-Hill Publishers, New York, 1996, pp. 6.1–6.62.
[56] E.M.V. Hoek, M. Elimelech, Cake-enhanced concentration polarization: a new fouling mechanism for salt-rejecting membranes, Environ. Sci. Technol. 37 (2003) 5581–5588.
[57] M. Herzberg, M. Elimelech, Biofouling of reverse osmosis membranes: role of biofilm-enhanced osmotic pressure, J. Membr. Sci. 295 (2007) 11–20.
[58] Z.E. Hughes, J.D. Gale, Molecular dynamics simulations of the interactions of potential foulant molecules and a reverse osmosis membrane, J. Mater. Chem. 22 (2012) 175–184.
[59] W.-Y. Ahn, A.G. Kalinichev, M.M. Clark, Effects of background cations on the fouling of polyethersulfone membranes by natural organic matter: experimental and molecular modeling study, J. Membr. Sci 309 (2008) 128–140.
[60] D.T. Myat, M.B. Stewart, M. Mergen, O. Zhao, J.D. Orbell, S. Gray, Experimental and computational investigations of the interactions between model organic compounds and subsequent membrane fouling, Water Res. 48 (2014) 108–118.
[61] G.-Y. Chai, W.B. Krantz, Formation and characterization of polyamide membrane via interfacial polymerization, J. Membr. Sci. 93 (1994) 175-l 92.
[62] J. Robertson, T. Centeno-Hall, A. Padias, R. Bates, H. Hall, Kinetics of model reactions for interfacial polymerization, Polymers 4 (2012) 741–746.
[63] C. Bissantz, B. Kuhn, M. Stahl, A medicinal chemist's guide to molecular interactions, J. Med. Chem. 53 (2010) 5061–5084.
[64] M.D. Kiran, N.V. Adikesavan, O. Cirioni, A. Giacometti, C. Silvestri, G. Scalise, R. Ghiselli, V. Saba, F. Orlando, M. Shoham, N. Balaban, Discovery of a quorum-sensing inhibitor of drug-resistant Staphylococcal infections by structure-based virtual screening, Mol. Pharmacol 73 (2008) 1578–1586.
[65] P. Dauber-Osguthorpe, V.A. Roberts, D.J. Osguthorpe, J. Wolff, M. Genest, A.T. Hagler, Structure and energetics of ligand binding to proteins: *E. coli* dihydrofolate reductase-trimethoprim, a drug-receptor system, Proteins: Structure, Function and Genetics 4 (1988) 31–47.